

Composite Elastomer Exhibiting a Stress-Dependent Color Change and High Toughness Prepared by Self-Assembly of Silica Particles in a Polymer Network

Eiji Miwa, Kenta Watanabe, Fumio Asai, Takahiro Seki, Kenji Urayama, J r my Odent, Jean-Marie Raquez, and Yukikazu Takeoka*



Cite This: *ACS Appl. Polym. Mater.* 2020, 2, 4078–4089



Read Online

ACCESS |



Metrics & More

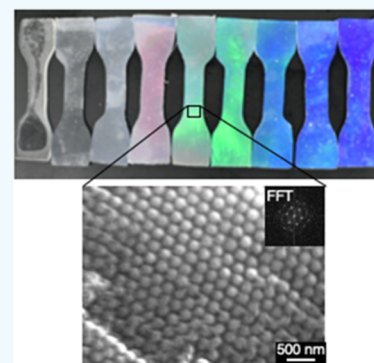


Article Recommendations



Supporting Information

ABSTRACT: In this study, we developed a composite elastomer exhibiting both mechanical toughness and a structural color change using submicron-sized spherical fine silica particles with a uniform size as fillers and arranging them in a periodic structure in the elastomer. In this composite elastomer, the fine silica particles formed colloidal crystals in a nonclosest-packed state, so that the composite elastomer was very flexible. We showed the possibility for use as strain and stress sensors that can measure the amount of strain applied to and the stress generated in the composite elastomer according to the position of the reflection peak produced by the composite elastomer. In this composite elastomer, both the fracture stress and the fracture strain were improved by increasing the amount of fine silica particles so that the fracture energy and toughness increased. As a result, the fracture energy of the composite elastomer containing 35 vol % fine silica particles was 13.5 times that of the system containing no fine silica particles. In the stress–strain curve observed by uniaxial stretching of this composite elastomer, a shoulderlike change was observed at different positions depending on the content of the fine silica particles, and further stretching resulted in a large energy dissipation. It was also found that after being strained beyond the shoulder position for the composite elastomer containing 44.9 vol % fine silica particles, the composite elastomer became tougher than before it was stretched. This composite elastomer may be toughened by a change in the interaction between the silica–polymer interface that resulted from uniaxial stretching and a dissipation of the energy caused by a change in the particle arrangement. The composite elastomer developed by the present novel method has the ability to be toughened by being subjected to a large strain once and can be a safe material that can avoid sudden fracture.



KEYWORDS: composite elastomer, structural color, toughness, nonclosest-packed colloidal crystal, fine silica particle, strain and stress sensor

1. INTRODUCTION

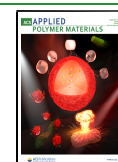
In general, the mechanical properties of polymer materials with a Young's modulus lower than that of metals and ceramics were improved by compounding them with a hard filler.^{1,2} For example, tires used for automobiles and airplanes are made by adding a large amount of carbon black or fine silica particles as a filler into natural rubber or synthetic rubber to carry out cross-linking. As a result, in addition to cross-linking and entanglement of polymer chains in the tire, various hierarchical structures are formed, such as a polymer adsorbed layer that is adsorbed at the filler interface and has a reduced mobility and a network structure in which the fillers are connected. As a result, a composite with a high toughness is achieved. To support heavy objects, such as automobiles and aircraft, most tires contain as much as 20–40% carbon black in the tire. Many people recognize that the color of a tire is black because of the color of the carbon black mixed in the tire. If fine silica particles are used as the main filler, the tire becomes white due to the influence of the color of the fine silica particles. That is,

the color of a composite elastomer in which a large amount of filler is used is influenced by the color of the filler. If the filler can be used in a composite elastomer to form a submicron-sized ordered structure, the resulting composite elastomer will exhibit a vivid interference color (structural color) due to the ordered structure.^{1,3–14} That is, depending on the type of filler and the state of dispersion of the filler in the elastomer, it becomes possible not only to improve the mechanical performance of the composite elastomer but also to impart optically interesting properties. It has been reported so far that a composite elastomer displaying a vivid structural color can be obtained by arranging monodisperse spherical fillers in an

Received: June 29, 2020

Accepted: July 31, 2020

Published: August 3, 2020



ordered state in an elastomer. However, most of these studies focus on the structural color development of a composite elastomer, and few studies focus on the mechanical properties of a composite elastomer that has such an ordered structure.

Here, we studied a composite elastomer exhibiting both mechanical toughness and structural color expression using submicron-sized spherical fine silica filler particles with a uniform particle size and arranging them in a periodic structure in the elastomer. To make the composite elastomer flexible, we adopted a non-close-packed state in which the fillers did not directly contact each other in the elastomer. To arrange the submicron-sized particles in a non-close-packed and ordered state, it was advantageous to have a repulsive force between the particles.¹⁵ We used a system in which electrostatic repulsion occurred between the particles. When fine silica particles with dissociative silanol groups on the surface are dispersed in a liquid monomer di(ethylene glycol) methyl ether methacrylate (MEO₂MA) at room temperature, the surface of the fine silica particles becomes charged negatively (Figure 1a).¹⁶ Mono-dispersed spherical fine silica particles (hereinafter referred to

as silica particles) were dispersed in MEO₂MA containing a small amount of cross-linking agent, and nonclose-packed colloidal crystals were formed by electrostatic interactions. By polymerizing the suspension, the nonclose-packed colloidal crystals were immobilized in the cross-linked network. As a result, a transparent composite elastomer that displayed a vivid color was obtained by reflecting a specific wavelength of visible light by Bragg reflection. The spacing of the silica particles in this composite elastomer changed with the deformation of the elastomer matrix so that the structural color that developed also changed. As a result, it was clarified that this elastomer can be used as a sensor that detects the amount of strain applied to it and the stress value at that time because of a change in its color. It was also found that the silica particles also functioned as fillers in the elastomer and improved the mechanical strength of the elastomer. In general, increasing the rigidity of an elastomer by increasing its cross-link density usually comes at the expense of its extensibility.^{17,18} This is because the short polymer strands between cross-links limit the flexibility of the structure. Even in a system in which a filler is mixed with a general polymer cross-linked body, the rigidity is increased depending on the amount of the filler, but the extensibility is deteriorated.¹⁹ However, it was demonstrated that our system had an improvement in both the rigidity and the extensibility of the elastomer with increasing silica particle content, resulting in an increase in the toughness. Using various evaluation methods, we investigated the mechanism by which submicron-sized, monodispersed spherical fine silica particles increased the toughness after being combined with a cross-linked MEO₂MA.

2. RESULTS AND DISCUSSION

2.1. Preparation of the Composite Elastomer.

In this study, various amounts of powdered silica particles were mixed in the solutions that contained a mixture of MEO₂MA and poly(ethylene glycol) dimethacrylate (PEGDMA), a cross-linking agent, at a ratio of 1000:1. Although silica particles with an average particle diameter of 179 nm were used, for comparison, silica particles with average particle diameters of 150, 210, 239, and 302 nm (Table S1) were also used. The following is a description of the composite elastomers prepared using the 179 nm silica particles, unless otherwise noted. An ultrasonic homogenizer was used to disperse the silica particles in the monomer solution. In the MEO₂MA, the ζ -potential of the silica particles was -31 mV (Table S3), and the silica particles were negatively charged and covered with positive charges. Therefore, a repulsive force was generated when the silica particles came close to each other. In a suspension containing less than 10.5 vol % silica particles, the silica particles were dispersed in a disordered state in the suspension, so the suspension became cloudy due to Mie scattering from the silica particles (Figure 1b). When the amount of silica particles in the suspension increased, the electrostatic interaction between the silica particles increased, and the silica particles formed an ordered arrangement. As a result, the suspension was colored with various hues depending on the amount of silica particles (Figure 1b).²⁰ Azobis(isobutyronitrile) (AIBN) was added to the suspension as an initiator, and the suspension was enclosed in a simple cell (Figure S13) with a thickness of 1 mm. A composite elastomer was prepared by free radical polymerization at 70 °C for 15 h. Since the system contracted with the polymerization of the monomer, the amount of silica particles in the obtained composite elastomer

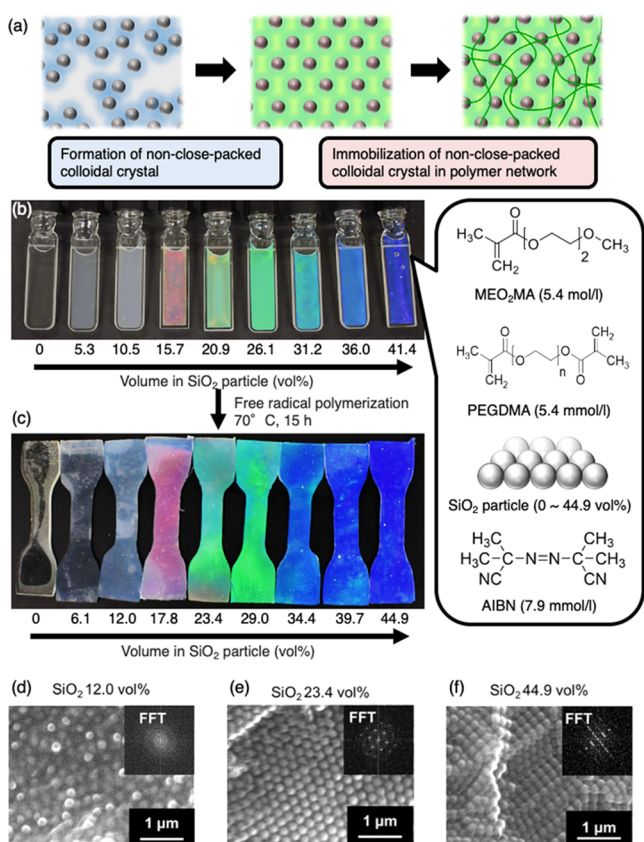


Figure 1. (a) Conceptual diagram in which charged monodispersed fine particles in a monomer solution form a nonclose-packed colloidal crystal and are fixed by polymerization. (b) Photograph of suspensions of monodispersed silica particles with various volume fractions in MEO₂MA solution containing poly(ethylene glycol) dimethacrylate (PEGDMA) and azobisisobutyronitrile (AIBN). In the suspensions with 15.7 vol % or more, the silica particles formed a colloidal crystal in a nonclose-packed state, thereby exhibiting a structural color. (c) Photograph of the elastomers obtained by polymerizing the suspension of (b). (d–f) Scanning electron micrographs of the cross sections of the elastomers with different silica particle contents: (d) 12 vol %, (e) 23.4 vol %, and (f) 44.9 vol %.

is referred to as the volume fraction after polymerization (Figure 1c). By considering the volume fraction, the occupation rate of fine particles in a space can be known. Since the obtained composite elastomer maintained the ability to form vivid colors that appeared in the suspension, it was considered that the silica particles became fixed in the composite elastomer without largely breaking their arrangement.

By observing the cross section of the composite elastomer with an electron microscope, it was possible to confirm the arrangement of the silica particles (Figure 1d–f). In the cloudy composite elastomer containing 12.0 vol % silica particles, the silica particles seemed to be randomly arranged (Figure 1d). A Fourier transform of the scanning electron microscope (SEM) image revealed a halo pattern, indicating that the silica particles formed an isotropic array with a short-range order (Figure 1d inset).^{21,22} On the other hand, it was confirmed that the silica particles were in a periodically arranged state when the amounts of silica particles were 23.4 and 44.9 vol % (Figure 1e,f). In these composite elastomers, the silica particles formed a face-centered cubic (fcc) structure, and the surface of the composite elastomer mainly had a (111) preferred orientation.^{14,23,24} Therefore, the bright color observed in the suspension and the composite elastomer was a structural color derived from the Bragg reflection generated by the (111) plane of the fcc silica particles.

2.2. Sensor Utilizing Structural Color Development of the Composite Elastomer. Figure 2 shows photographs of composite elastomers with silica contents of 0, 17.8, 23.4, and 44.9 vol %. As shown in the photographs, when the content of silica particles in the elastomer made of the MEO₂MA polymer increased, the hardness of the composite elastomer increased, but the system containing 44.9 vol % silica particles was flexible. The elastomer without silica particles was colorless and transparent (Figure 2a). The composite elastomer containing 17.8 vol % silica particles was red and slightly cloudy (Figure 2b). At 23.4 vol %, it became green, and the transparency increased slightly (Figure 2c). Furthermore, at 44.9 vol %, it turned blue and exhibited a high transparency (Figure 2d). As the color generated from the composite elastomer was a structural color, and since the composite elastomer transmitted light, the colors were vivid when the background was black.²⁵ However, when the background color was white, a vivid hue was difficult to observe with the naked eye because of the light that was reflected from the back surface.²⁶ The hue and transparency of the composite elastomers can also be understood from the transmittance spectra of the composite elastomers (Figure 2e). The transparency increased with the content of the fine particles because the fine particles were less disturbed and the scattered light was canceled by interference. It can be seen from the reflection spectrum that the light in a specific region was strongly reflected under the Bragg condition (Figure 2f). The peak wavelength caused by the Bragg reflection moved to a lower wavelength as the content of silica particles increased. The position λ_{\max} of this reflection peak is given by the following equation, assuming that the Bragg reflection was caused by the (111) plane in the fcc crystals:

$$\lambda_{\max} = \frac{2\sqrt{6}}{3} D \sqrt{n_a^2 - \sin^2 \theta} \quad (1)$$

In this formula, D is the center-to-center distance of the silica particles. Additionally, θ is the incident angle of light with

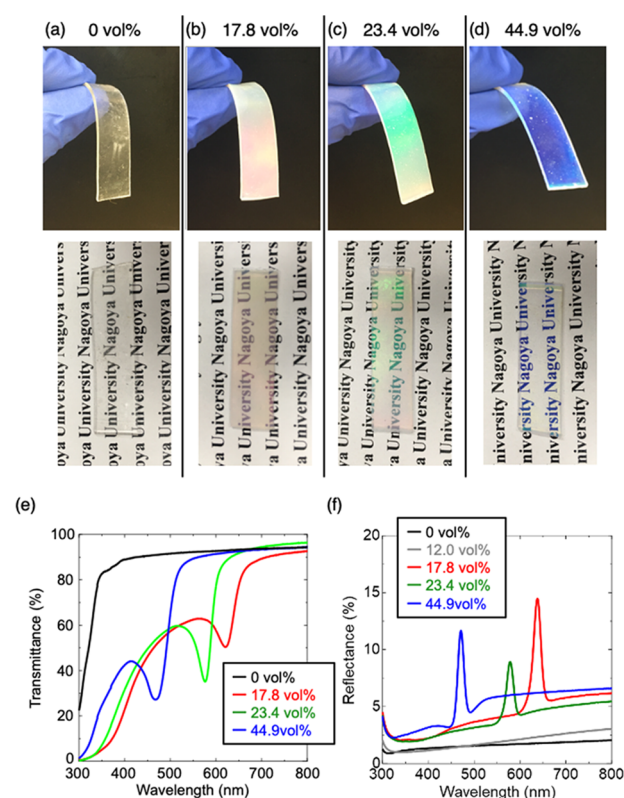


Figure 2. Optical properties of the elastomers consisting of the MEO₂MA polymer and various amounts of monodispersed silica particles with an average particle size of 179 nm. Optical photographs of (a) 0 vol % silica particles (black and white background), (b) 17.8 vol % silica particles (black and white backgrounds), (c) 23.4 vol % silica particles (black and white backgrounds), and (d) 44.9 vol % silica particles (black and white backgrounds). (e) Transmission spectra of the elastomers consisting of the MEO₂MA polymer and various amounts of monodispersed silica particles with an average particle size of 179 nm. (f) Reflectance spectra of the elastomers consisting of the MEO₂MA polymer and various amounts of monodispersed silica particles with an average particle size of 179 nm.

respect to the direction perpendicular to the surface of the elastomer (Figure S1). Also, n_a is the average refractive index of the composite elastomer and is calculated by the following formula based on the refractive index n_i and the volume fraction ϕ_i of the constituent component 1:

$$n_a^2 = \sum n_i^2 \phi_i \quad (2)$$

The refractive indices of the silica and MEO₂MA polymer were set at 1.46 and 1.49 (Figure S19), respectively, and the values of D were calculated to be 267, 243, and 198 nm from the peak positions of the reflection spectra using eqs 1 and 2 for silica particle contents of 17.8, 23.4, and 44.9 vol %, respectively. Therefore, considering the particle size of 179 nm, the distances between the particle surfaces for silica particle contents of 17.8, 23.4, and 44.9 vol % were 88, 64, and 19 nm, respectively, in each composite elastomer. From the above, we could fabricate flexible composite elastomers exhibiting a full color range from red to blue by constructing a nonclose-packed colloidal crystal in which the amount of silica particles and the period interval were varied in the elastomers.

A change in structural color with uniaxial extension of the composite elastomer was observed. Here, the results of using a composite elastomer containing 23.4 vol % silica particles and

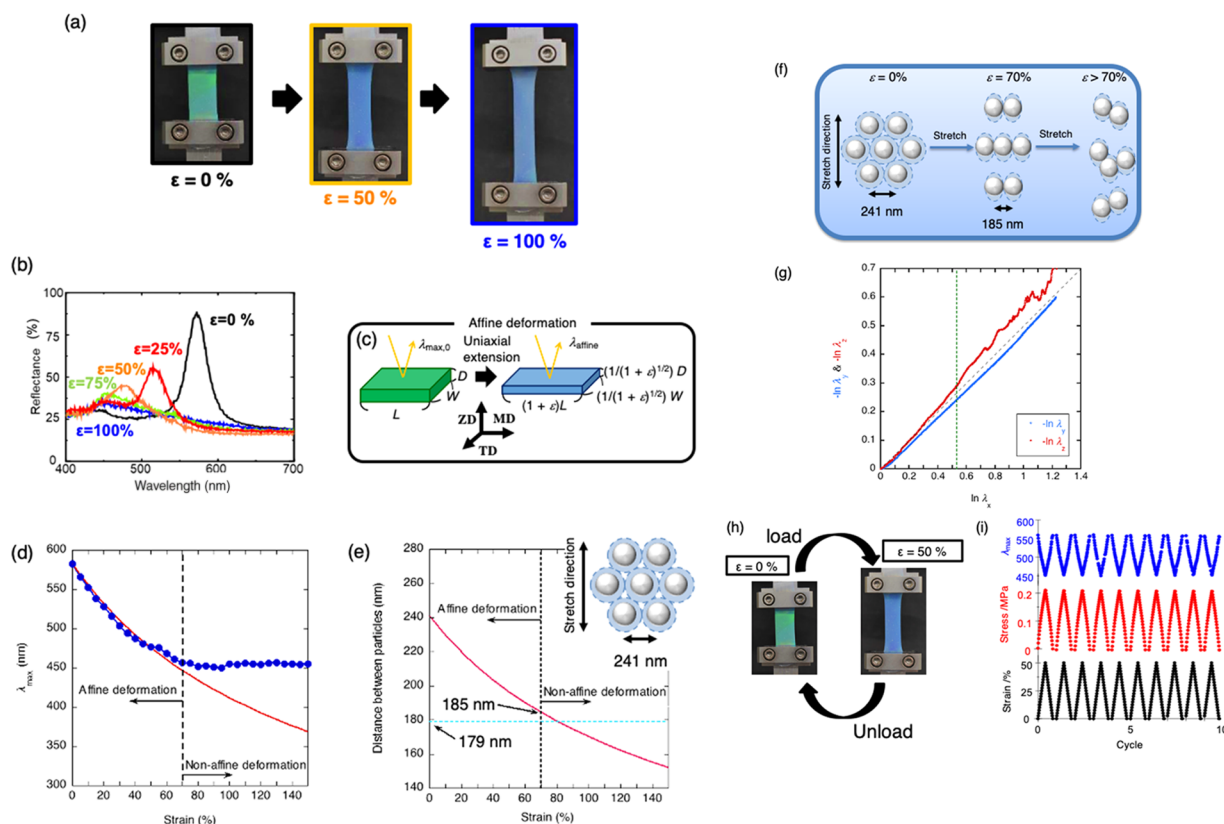


Figure 3. Change in structural color due to uniaxial stretching of a composite elastomer containing 23.4 vol % silica particles: (a) structural color observed at 0–100% strain and (b) reflection spectra observed when the distortion amount was 0–100%. (c) Relationship between the amount of strain and the size at the time of deformation when an affine deformation of the elastomer is assumed. (d) Relationship between the peak wavelength of the reflection spectrum and the amount of strain observed when the composite elastomer is uniaxially stretched, where the solid red line is the calculated value assuming affine deformation. (e) From the results of (d), a diagram showing the relationship between the amount of strain and the surface spacing between the fine particles is obtained using formula 1 and formula 2. The light-blue dotted line indicates the size of the fine particles used. Inset: colloidal crystal forming a face-centered cubic lattice structure with a nonclose-packed structure. (f) Conceptual diagram for predicting the change in the alignment state of the silica particles with the elongation of the composite elastomer. (g) Changes in Poisson's ratio in the film width direction and the film thickness direction with the uniaxial extension. The green dotted line indicates the position where the strain value is 70% due to the uniaxial extension in the x -axis direction. The black dotted line in the graph indicates a Poisson's ratio of 0.5. (h) Photographs of the composite elastomer with no strain and 50% strain. (i) Relationship between the peak value (λ_{\max}) of the reflection spectrum and stress and strain observed when reversibly changing the strain applied to the composite elastomer from 0 to 50%.

colored green in an unstretched state are shown. Figure 3a,b shows the results of the color change and reflectance spectra of the uniaxially stretched composite elastomer, respectively. The uniaxial stretching caused the composite elastomer to change the color from green to blue, and when the amount of deformation increased, the color development gradually disappeared (Figure 3a). As the composite elastomer was deformed, the reflection peak observed in the reflection spectrum shifted to a shorter wavelength and the intensity decreased (Figure 3b). Assuming an affine deformation in which the deformation of the colloidal crystal matched the deformation of the composite elastomer (Figure S26), the position of the reflection peak (λ_{affine}) caused by the affine deformation can be calculated by the following formula from the position of the reflection peak ($\lambda_{\text{max},0}$) observed without deformation and a given strain ε (Figure 3c)²⁷

$$\lambda_{\text{affine}} = \frac{1}{\sqrt{1 + \varepsilon}} \lambda_{\text{max},0} \quad (3)$$

Figure 3d shows the result of plotting the position (λ_{max}) of the observed reflection peak with the elongation of the composite elastomer and the position of the peak in the case of affine

deformation obtained from eq 3 against the strain amount. When the strain amount reached 70%, the position of the reflection peak obtained from the experiment showed good agreement with the expected affine deformation. However, when the strain amount exceeded 70%, the peak value became a constant value, and only the peak intensity decreased. One of the reasons why the shift of the peak position showed two different behaviors is that an increase in the repulsive force between the silica particles in the composite elastomer due to uniaxial stretching influenced the shrinkage in the film thickness direction or the film width direction. When the amount of strain was small, there was sufficient spacing between the silica particles, and the film thickness and film width contraction that accompanies the stretching easily occurred. However, when the amount of strain increased and the shrinkage of the film thickness and film width increased, the silica particles approached each other, and the repulsive force increased, which might have suppressed further shrinkage along the film thickness or film width directions. When the elastomer was uniaxially stretched assuming affine deformation, the adjacent particles came close to each other and a repulsive force was generated for the particles aligned in the film width

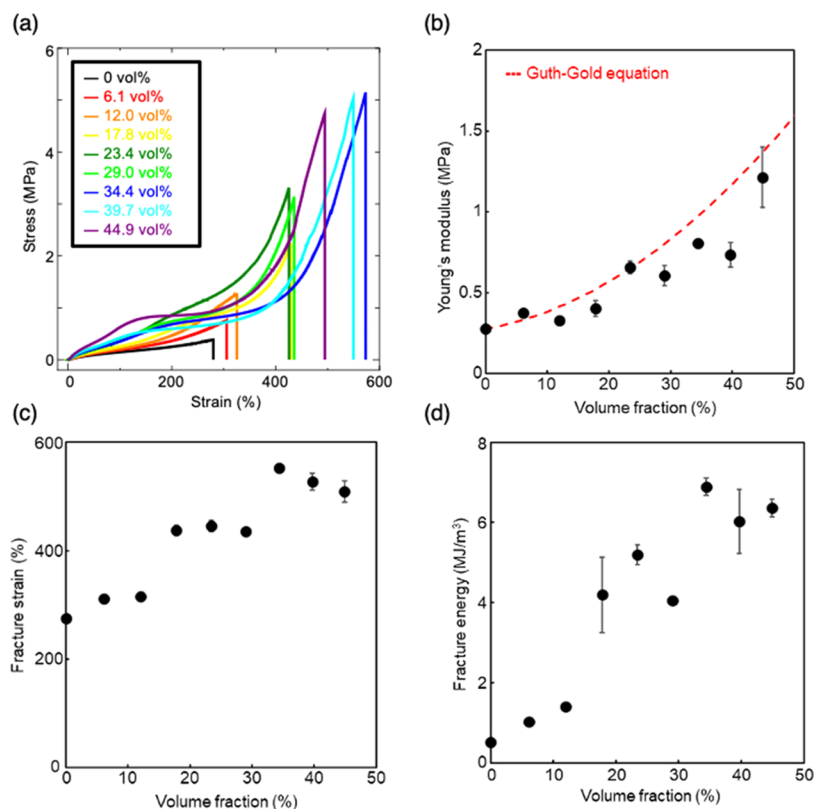


Figure 4. (a) Stress–strain test results of composite elastomers containing various amounts of monodispersed silica particles with an average particle size of 179 nm. (b) Diagram showing the relationship between the Young's modulus and the volume fraction of fine silica particles obtained from the result of (a). (c) Diagram showing the relationship between the fracture strain and the volume fraction of fine silica particles obtained from the result of (a). (d) Diagram showing the relationship between the fracture stress obtained from the result of (a) and the volume fraction of fine silica particles.

direction, according to the simulation results (Figure S27). That is, the particles present in the plane contacted each other earlier than the particles present in the direction perpendicular to the observation surface of the reflection spectrum. For example, when the nonclosest-packed colloidal crystals that formed a face-centered cubic lattice with respect to the stretching direction of the elastomer were arranged as shown in the inset in Figure 3e (Figure S28), the relationship between the particle distance and the strain value was as shown by the red solid line in Figure 3e, assuming affine deformation. However, the distance between the particles was 185 nm when the strain amount was 70%, according to the red solid line. Since the particle size of the silica particles was 179 nm, the distance between the surfaces of the particles was 6 nm when the strain amount was 70%. Considering that the silica particles were charged and the polymer was adsorbed on the surface of the silica particles, it is appropriate to consider that the silica particles were not brought closer to each other. However, it is clear from the photograph in Figure 3a that even if the strain amount exceeded 70%, the composite elastomer actually contracted in the film width direction. From these results, it can be inferred that when the strain amount reached 70% or more, the arrangement of the fine particles arranged in the surface direction of the composite elastomer became disordered, as shown in Figure 3f. Figure 3g shows the true strains in the width (y) and thickness (z) directions as a function of that in the stretching (x) direction. The gradient corresponds to Poisson's ratio (μ),²⁸ and the black dotted line denotes the mechanically isotropic and incompressible

condition of $\mu = 0.5$. The linear approximations for the relations result in $\mu_y = 0.49$ and $\mu_z = 0.57$. The relation $\mu_z > \mu_y$ indicates that lateral shrinkage occurs anisotropically, whereas the volume is preserved ($\mu_y + \mu_z \approx 1$). The shrinkage in the thickness direction is larger than that in the width direction. From the above, it can be seen that the arrangement of the fine particles was disturbed as the composite elastomer was stretched. However, since the short-range order of the fine particles may have existed, coherent scattering of the light due to the short-range order may have been observed even in the composite elastomer with a strain of 70% or more.^{22,29} As a result, it is considered that λ_{\max} became a constant value, as shown in Figure 3d.

From the above, it was clarified that the macroscopic deformation of the composite elastomer can be quantitatively evaluated by observing the reflection spectra when the strain amount reaches 70%. However, it was considered that the macroscopic deformation of the composite elastomer could not be evaluated by the reflection spectra when the strain amount was 70% or more because the arrangement of the fine particles in the composite elastomer can be disturbed. Therefore, to use this elastomer with a content of 23.4 vol % silica particles as a sensor, it is appropriate to use it up to 70% strain with a clear color change. When the strain amount reaches 50%, the elastomer exhibits rubber elasticity and reversibly deforms without a residual strain, so the change in the peak position of the reflection spectrum is reversible (Figure 3h). Since the relationships among the amount of strain applied to the elastomer, the stress generated in the

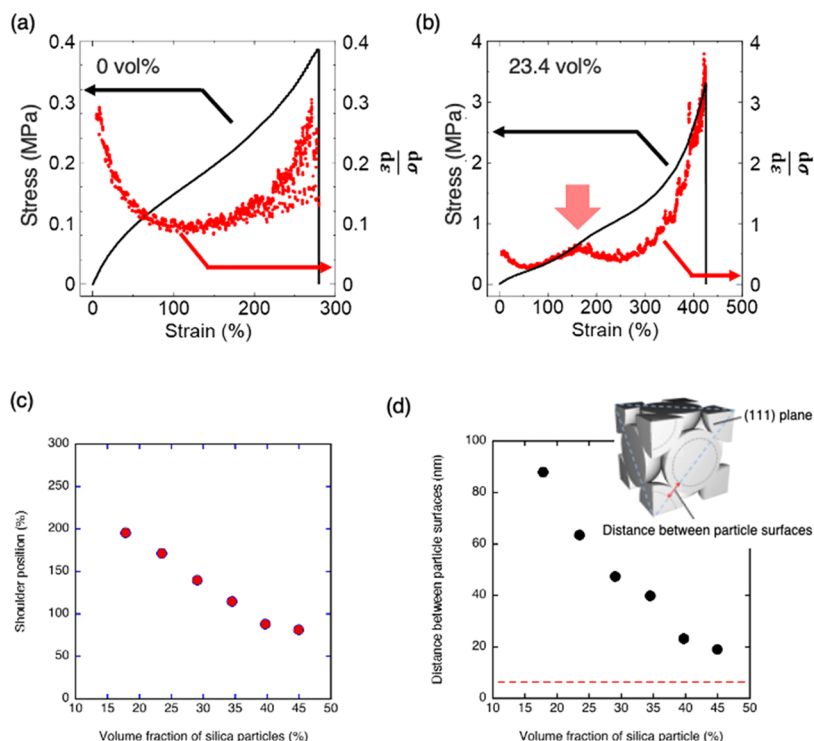


Figure 5. (a) Elastomer stress–strain curve and its differential function in the case of the elastomer with no shoulder on the stress–strain curve. (b) Stress–strain curve of an elastomer with a shoulder and its differential function. (c) Diagram showing the relationship between the shoulder position in the stress–strain curve and the volume fraction of the silica particles. (d) Diagram showing the relationship between the surface distance of the silica particles and the volume fraction of the silica particles. The red line shows the distance between the surfaces of the silica particles (6 nm) when the volume fraction is 23.4 vol % and 70% and a strain was applied during uniaxial stretching. The inset shows the same state in Figure 3e as a unit cell.

elastomer, and the position of the reflection peak at that time repeatedly matched (Figure 3i), the elastomer can be applied as a strain sensor or a stress sensor.^{7,13} If a system is needed that exhibits a reversible response in a range of color changes and strain amounts, then the amount of silica particles and the size of silica particles must be changed (see the Supporting Information).

2.3. Increased Toughness of the Composite Elastomer. **2.3.1. Uniaxial Elongation Test.** There is a trade-off between the hardness and flexibility of general elastomers (Figure S25).¹ In this study, we found that the composite elastomer had an improved Young's modulus and fracture strain, and the toughness increased as the amount of silica particles added increased. Figure 4 shows the results of the stress–strain test by uniaxial elongation that was done to investigate the mechanical properties of the composite elastomer. The Young's modulus obtained from the stress–strain curve in Figure 4a increased as the amount of silica particles in the composite increased, which is consistent with the relationship shown by the Guth–Gold equation indicated by the red dashed line (Figure 4b). The Guth–Gold equation is a classical expression for the elastic modulus of filler reinforced elastomers, which is obtained as an extension of the Einstein viscosity equation for spherical rigid particle suspensions:

$$E^* = (1 + 2.5\phi + 14.1\phi^2)E \quad (4)$$

where E^* and E are Young's moduli of the filled and unfilled elastomers, respectively, and ϕ is the volume fraction of the silica particles. In many filled elastomers, E^* tends to exceed

significantly the expectation of eq 4 in the high ϕ region, and the deviation has been attributed to the formation of finite aggregates.³⁰ The agreement of E^* of the present composite elastomers with eq 4 in a wide ϕ range suggests the dispersion of the silica particles without appreciable aggregation.

Additionally, the fracture strain increases with increasing silica particle loading (Figure 4c). The elastomer that did not contain a filler fractured at a strain value of 300% or less, whereas the strain value was extended to 500% or more by adding silica particles. In a conventional composite elastomer, the Young's modulus is often increased by adding a filler, but it is rare that the extensibility is improved.² However, the fracture strain value reached a maximum when the amount of silica particles was approximately 35 vol % (also see Figure S38a), and the fracture strain value decreased as the amount of silica particles further increased. When the amount of silica particles increased to 35 vol % or more, the ratio of the flexible matrix layer decreased, which decreased the flexibility of the composite elastomer. When the amount of silica particles reached 35 vol %, both the Young's modulus and the fracture strain of the composite elastomer improved, and the fracture energy required to fracture the composite elastomer increased (Figure 4d). As a result, the fracture energy of the composite elastomer containing 35 vol % silica particles was 13.5 times that of the system that contained no silica particles. Combining simultaneous improvements in stiffness, toughness, and extensibility is a typical challenge of conventional (nano)-composites with only very few limited successes in the field. Among them, Odent et al. developed ultrastretchable and tough ionic nanocomposites without the associated property

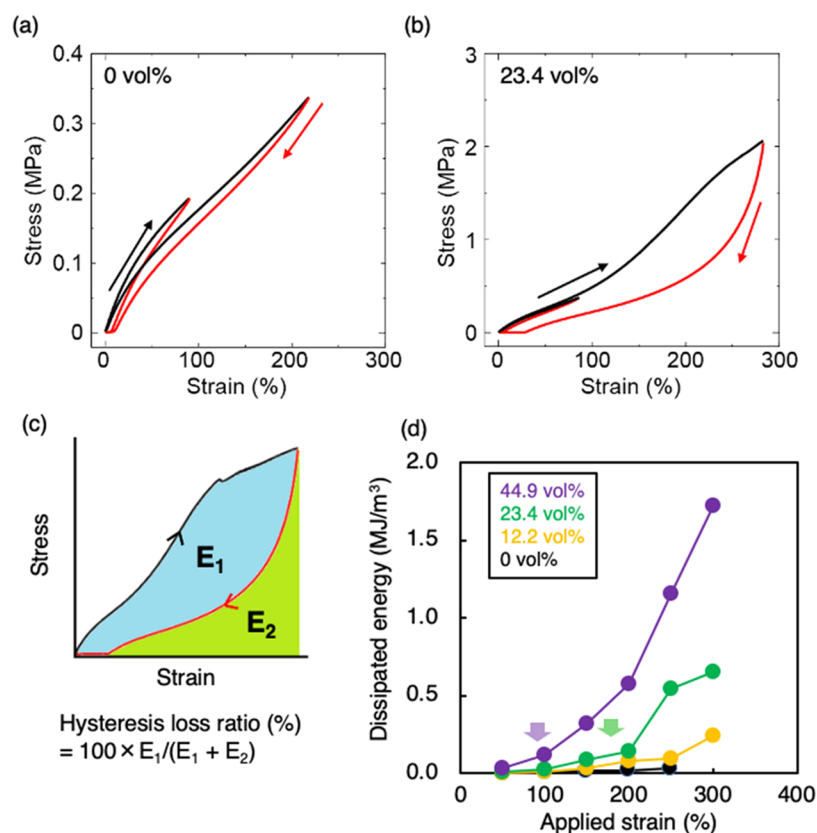


Figure 6. (a) Hysteresis test of the elastomer with 0 vol % silica content. (b) Hysteresis test of the elastomer with 23.4 vol % silica content. (c) Diagram showing the calculation method of the hysteresis loss rate. (d) Diagram showing the relationship between dissipated energy and the applied strain amount of elastomers with different fine silica particle contents.

trade-offs, which was the result of maximizing electrostatic interactions in the system.^{31–33}

A characteristic of the stress–strain curves of this system is that shoulders are seen for strain values from 100 to 200% in the composite elastomer with a silica particle content of 17.8 vol % or more. Focusing on this shoulder, we investigated the reinforcing mechanism of the filler. To investigate the position of the shoulder on the stress–strain curve, the stress was differentiated with respect to the strain value, and a change in the gradient of the stress–strain curve was obtained. Elastomers without silica particles behaved similarly as general rubber (Figures 5a and S26). On the other hand, since the shoulder appeared in the stress–strain curve of the composite elastomer containing silica particles, a peak is seen in the differential curve (Figure 5b). When this peak position was taken as the shoulder position and plotted against the volume fraction of the silica particles, it can be seen that the shoulder appeared in the low strain region as the amount of silica particles increased (Figure 5c). The relationship between the surface distance and the volume fraction of the silica particles obtained using eqs 1 and 2 is shown in Figure 5d and was based on the value of the peak in the reflection spectrum observed for composite elastomers that had different silica particle contents. Judging from the results in Figure 3, the following two processes seemed to occur mainly before the shoulder occurred during uniaxial elongation of the composite elastomer. For the composite elastomer containing 23.4 vol % silica particles, when a 70% strain was applied by uniaxial stretching, the silica particles in the composite elastomer approached each other until they made contact (from the

results in Figure 3e, the distance between the two surfaces was up to 6 nm, which is indicated by the red dotted line in Figure 5d). When the composite elastomer was further stretched, the silica particles in the composite elastomer formed aggregates with a short-range order, but their arrangement was disturbed (Figure 3f), and the shoulder occurred when the strain amount reached 172% (Figure 5c). This means that the shoulder is linked to the moment the silica arrangement is disturbed. However, we found from the following experiment that the toughness of the composite elastomer was affected by the phenomenon that occurred after the shoulder appeared rather than before the shoulder appeared.

2.3.2. Hysteresis Loss Rate Measurement. Composite elastomers containing 17.8 vol % or more of the silica particles have a shoulder in their stress–strain curve, and there is likely a mechanism to relax the strain energy when large deformations occur. Therefore, the rate of energy dissipation of the elastomer was evaluated by changing the amount of strain applied and measuring the hysteresis loop.

Elastomers not filled with silica particles demonstrated little hysteresis regardless of the amount of strain applied, and the stress–strain curve during the unloading process passed just below the loading process (Figure 6a). On the other hand, an elastomer composed of 23.4 vol % silica particles exhibited a behavior with less hysteresis when the applied strain amount was 100%, similar to that for the elastomer that did not contain a filler. However, when the strain amount was approximately 300% beyond the position where the shoulder occurred, a large hysteresis occurred (Figure 6b). Figure 6d shows the dissipation energy calculated from the area ratio of the

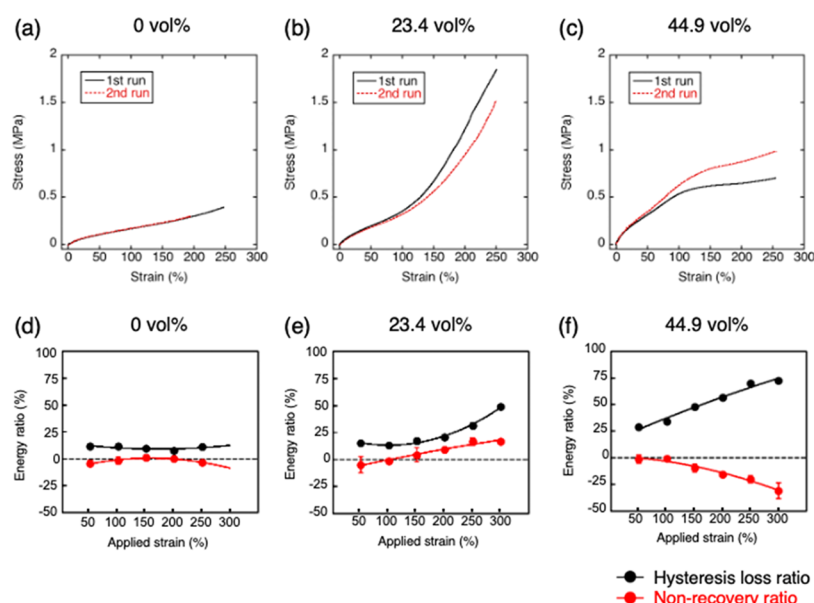


Figure 7. Stress–strain curves when elastomers with different fine silica particle contents were given a certain amount of strain and then strained completely again for (a) silica particle content of 0 vol %, (b) silica particle content 23.4 vol %, and (c) silica particle content of 44.9 vol %. (d–f) From the results of (a)–(c), the diagram was obtained by obtaining the energy recovery rate of the test piece and plotting it against the applied strain amount.

stress–strain curve during loading and unloading (Figure 6c). In a composite elastomer with a small number of silica particles, the dissipated energy became constant regardless of the amount of strain applied. On the other hand, in the composite elastomer containing 23.4 vol %, the dissipated energy increased significantly above a strain of approximately 200%. In the composite elastomer containing 44.9 vol % silica particles, the dissipated energy increased above a strain amount of approximately 100%. Considering the shoulder positions discussed above, it is clear that the strain values at which the dissipated energy began to increase occurred after the shoulders appeared. Per the discussion above, it is suspected that the elastomers containing a large amount of silica particles were toughened due to energy that was dissipated during the friction between particles that was caused by a change in the interaction between silica–polymer interfaces and in the arrangement of the silica particles.

2.3.3. Energy Recovery Rate Measurement. Figure 7a–c shows the results of two uniaxial elongation tests for one sample at a maximum strain of 250%. For the MEO₂MA elastomer that does not contain silica particles, the first and second test results overlapped regardless of the applied strain amount, and no permanent hysteresis was seen (Figure 7a). In other words, it can be said that the hysteresis loss exhibited by the MEO₂MA matrix alone was due to the reversible energy dissipation. Similar results were obtained for the composite elastomer containing 12.2 vol % or fewer silica particles in which no shoulder was observed on the stress–strain curve.

On the other hand, from 17.8 to 29.0 vol % in which the shoulder appeared during the uniaxial elongation test, when a 250% strain that exceeds the shoulder region is applied, a stress value lower than what occurred during the first elongation appeared during the second elongation (Figure 7b). Interestingly, as the amount of silica particles was increased, the recovery rate after relaxation increased, and the system containing 44.9 vol % silica particles clearly showed an elevated stress value during the second elongation (Figure 7c).

The same measurement was performed on the test pieces to which other strain amounts were given, and the hysteresis loss rate and the energy rate that did not recover during the second extension were obtained (Figures 7d–f, S67, and S69). In the case of the MEO₂MA elastomer and the composite elastomer with silica particle contents of 6.1 and 12.0 vol %, the energy rate that was not recovered was approximately 0% regardless of the applied strain. In other words, the energy that was dissipated during the first extension was completely restored by the relaxation process. On the other hand, in the systems where the amounts of silica particles were 17.8, 23.4, and 29.0 vol %, the hysteresis loss rate increased when the strain value exceeded the shoulder region, and the amount of energy that was dissipated that did not recover after relaxation also increased. However, the recovery rate after relaxation increased when the amount of silica particles in the composite increased, and in the system with 44.9 vol % silica particles, the second unrecovered energy rate clearly showed a negative value. In other words, we found that the toughness was higher than that before the deformation. In our previous research, when a composite elastomer containing 34 vol % silica particles in a cross-linked MEO₂MA polymer was stretched above the strain value at which a shoulder appeared, the change in the fcc structure formed by the silica particles remained after stretching.¹⁶ If the stress relaxed due to the change in the interaction with the polymer matrix that was adsorbed on the surface of the silica particles when the composite was stretched above where the shoulder appeared, then it is suspected that the arrangement of the silica particles was greatly disturbed and not restored. As a result, in the composite elastomer filled with a high concentration of silica particles, the toughness of the composite elastomer might have increased during elongation due to the deformation of the colloidal crystal structure.

3. CONCLUSIONS

By fixing the colloidal crystals formed by the silica particles in a flexible elastomer, a composite elastomer that exhibited a full color range from red to blue was prepared and depended on the number of silica particles. The composite elastomer can be applied as a sensor because the amount of strain due to uniaxial stretching vividly changes its color depending on the amount of stress and strain. We also found that the Young's modulus and elongation of the composite elastomer increased with the addition of silica particles up to 35 vol %. As a result, the composite elastomer was toughened by the addition of silica particles. It can be suggested from the measurement of the dissipated energy and hysteresis loss rate that the existence of a shoulder in the stress–strain curves indicated toughening of the composite elastomer. It was also shown that in the system containing 44.9 vol % silica particles, when a strain exceeding the position of the shoulder was applied by uniaxial extension, a larger stress was generated when the extension was performed again. It is presumed that the change in the arrangement of the silica particles introduced into the composite elastomer increased the toughness of the composite elastomer by enabling an elongation beyond the shoulder. Sudden fracture of elastomers during use is a safety concern. A system, such as the composite elastomer developed by the present novel method, has the ability to be toughened by being subjected to a large strain once and can then ensure safe operation during use. Also, if the force applied to the elastomer is removed after it has been greatly stretched beyond the shoulder, the elastomer exhibits a structural color depending on the recovered size. In other words, the history of large distortion is shown as a change in structural color.

Since this system is optically transparent, it became possible to observe the internal static and dynamic microstructures using a confocal microscope. By observing the dynamic behavior of the silica particles and microstructure when the composite elastomer was strained, it was possible to investigate the details of the toughening mechanism of the composite elastomer upon the addition of a filler. Although details regarding the improvement in the extensibility of the composite elastomer by the addition of silica particles are not known, the extensibility may be a result of the polymer formation reaction that occurs when the particles are tightly packed, which affects the conformation of the obtained polymer. By conducting these verifications, a new toughening mechanism of the composite elastomer will become clear. Understanding the mechanism of material toughness is important because it leads to the development of a safe material that can avoid sudden fracture.

4. EXPERIMENTAL SECTION

4.1. Materials. Di(ethylene glycol) methyl ether methacrylate (MEO₂MA) 95% (Sigma-Aldrich, density 1.02 mg/cm³, molecular weight 188.22 g/mol) was used as a monomer to prepare the elastomer, poly(ethylene glycol) dimethacrylate (PEGDMA) was used as a cross-linking agent (Sigma-Aldrich, density 1.10 mg/cm³, molecular weight 550 g/mol), and the initiator *N,N*-azobisisobutyronitrile (AIBN) (Kanto Kagaku, density 1.1 mg/cm³, molecular weight 164.21 g/mol) was used without purification. Monodispersed spherical silica particles with particle sizes of 150, 179, 210, 239, and 302 nm (Fuji Chemical, Silibol 150, Silibol 180, Silibol 210, Silibol 240, and Silibol 300, respectively) were used (Table S1). The density of the silica particles was 2.21 g/cm³. Tap water was purified and deionized with MILLI-Q Labo (MILLIPORE), and the electrical resistivity was adjusted to 18.2 MΩ·cm before use.

4.2. Preparation of Samples. **4.2.1. Preparation of the Silica Particle Composite Suspension.** After placing 2700 mg of MEO₂MA and 7.9 mg of PEGDMA in a test tube, 5.3, 10.5, 15.7, 20.9, 26.1, 31.2, 36.3, and 41.4 vol % silica particles with respect to the total volume of the suspension were added. Here, the molar ratio of MEO₂MA and PEGDMA was 1000:1. Then, the samples were ultrasonicated using a tabletop ultrasonic cleaner to loosen the agglomerates until precipitation of the silica particles did not occur. Subsequently, the suspensions were subjected to ultrasonication using an ultrasonic homogenizer (Hierascher, UP200St) to completely disperse the silica particles (Figures S2–S12).

4.2.2. Fabrication of the Simple Cell. A simple cell was used when polymerizing the suspension prepared by the above method to prepare an elastomer by the following procedure. First, a fluorinated ethylene propylene (FEP) film (Fron Industries, FEP adhesive sheet film 100 μm thick) was attached to one side of a slide glass substrate. After that, a 1 mm thick hard silicone rubber sheet (ASONE, SR0301) was used as a spacer, and it was sandwiched between two glass slides with the FEP film surface facing inside. Finally, the cell was fixed with a clip. Figure S13 shows a diagram of the created simple cell.

4.2.3. Preparation of the Silica Particle Composite Elastomer. AIBN (3.4 mg) was added to the suspension prepared by the above method and completely dissolved using a vortex. Since the suspension containing a large amount of silica particles had a high viscosity, bubbles were generated during the vortexing process and were trapped in the suspension. After decompressing with a bell jar vacuum pump to remove the air bubbles, the suspension was injected into the simple cell described above. The sample was left standing in a constant-temperature dryer (Yamato Scientific, DS410) set at 70 °C for 15 h to carry out free radical polymerization. Since the obtained elastomer had a high adhesiveness, it was removed from the cell and then both sides were attached to a poly(tetrafluoroethylene) (PTFE) film (Nichias, Naflon film) with a thickness of 50 μm.

4.2.4. Thermogravimetric Analysis (TGA) of the Silica Particle Composite Elastomer. The thermogravimetric analysis of the silica particle powder and the prepared elastomer was performed by a differential thermal/thermogravimetric simultaneous measuring device (DTG60, Shimadzu Corporation). The measurement started at 40 °C, and then the sample was heated to 530 °C at a heating rate of 20 °C/min and held at 500 °C for 1 h. The weight ratio of the silica particles in the elastomer was calculated from the weight change before and after measurement; see Figure S18 and Table S4.

4.2.5. Field Emission-SEM (FE-SEM) Observations of the Cross Sections of the Silica Particle Composite Elastomers. Elastomer cross sections were created according to the freeze-fracture method. The prepared elastomer was placed in a mortar, liquid nitrogen was poured over it, the elastomer was rapidly frozen, and then the elastomer was hit with a pestle to fracture it and form a cross section. The prepared sample was subjected to 5 nm osmium vapor deposition using an osmium plasma coater, and then the cross section near the surface of the elastomer was observed by FE-SEM.

4.2.6. Optical Photography. A digital camera (Nikon, D3400) was used to take optical photographs of all samples.

4.2.7. Particle Size Measurement of the Silica Particles. The average particle size and the CV value of the silica particles used in this study were measured by a dynamic light scattering measuring device (Malvern, Zetasizer nano ZS) and a disk centrifugal-type particle size distribution measuring device (CPS Disc Centrifuge DC24000 UHR). Although the values obtained by both were different (Table S1), the values obtained by the disk centrifugal particle size distribution analyzer were used in this paper.

4.2.8. ζ-Potential Measurement of the Silica Particles. The ζ-potential of the silica particles was evaluated by the light scattering electrophoresis method. The sample was prepared by placing fine silica powder in a test tube with pure water or a solution diluted to 0.1 wt % with MEO₂MA and ultrasonicated in a tabletop ultrasonic cleaner (Branson CPX3800H-J). The sample with water as the solvent was placed in a disposable cell for ζ-potential (Malvern, DTS1070). The sample with MEO₂MA as the solvent was placed in a 12 mm

square glass cell (Malvern, PCS1115), and then, a universal dip cell (Malvern for the organic solvent, ZEN1002) was attached to the upper part, and the ζ -potential was measured by a particle size measuring device (Malvern, Zetasizer nano S) (Tables S2, S3).

4.2.9. Specular Reflection Measurement. The suspension spectrum under specular reflection (specular reflection) conditions and the reflection spectrum of the elastomer were measured. The measurement was performed in 10° steps from 10 to 60° so that the incident angle and the detection angle were equal to the vertical direction of the sample (Figure S1a).

4.2.10. Refractive Index Measurement. The results of previous studies on the refractive indexes of MEO₂MA, the MEO₂MA polymer, and silica particles were used (Figure S19). Each plot contains the measured value, and the broken line is the chromatic dispersion calculated using the Cauchy dispersion formula. Although the refractive index is dependent on the wavelength, in this study, we used n (MEO₂MA) = 1.44, n (MEO₂MA polymer) = 1.49, and n (SiO₂) = 1.46, which are the refractive indexes at 550 nm.

4.2.11. Transmission Spectrum Measurement. An ultraviolet–visible near-infrared spectrophotometer (JASCO, V-670) was used as a measurement device, and the sample installation and baseline/dark-line settings were performed in the same way as the absolute reflection spectrum measurement (see the Supporting information). A light source and a detector were installed in a straight line in the vertical direction with respect to the sample, and light passing through the sample was detected (Figure S20).

4.2.12. Regular Reflection Measurement during Elastomer Stretching. The reflection spectrum was measured while the elastomer was stretched to evaluate the discoloration characteristics associated with the deformation of the elastomer. A dynamic viscoelasticity measuring device (TA instrument, RSA-G1) was used to stretch the elastomer. Spectra Suite software manufactured by Ocean Optics was used for the reflection spectrum measurement device. A deuterium tungsten halogen lamp (Ocean optics, DH-2000-BAL) was used as a light source, and an ultrasensitive fiber multichannel spectrometer (Ocean Optics, QE65000) was used as a detector. In this measurement, the incident light and the detection were performed by the reflection terminal. The test piece was cut into a strip with a width of 10 mm using a straight cutter (dumbbell, SSPK-1000-D) and attached to the dynamic viscoelasticity measuring device so that the distance between the jigs was 20 mm. The specimen was stretched at an elongation rate of 3.0 mm/min, and the specular reflectance spectrum was measured at 2.5% strain intervals (Figure S21). The dark line with a reflectance of 0% was measured with the black plate blocking the detector, and the baseline with a reflectance of 100% was measured by placing an aluminum mirror plate perpendicular to the light source.

4.2.13. Regular Reflection Measurement with Cyclic Deformation. Considering the application of the elastomer as a sensor, it was necessary to show similar discoloration characteristics for repeated deformation cycles. Therefore, a strip-shaped test piece prepared using a straight cutter was attached to a dynamic viscoelasticity measuring device, and the specular reflection spectrum was measured by a reflection spectrum measurement device during repeated deformation. The test piece was stretched to a maximum strain of 50% at a stretching speed of 3.0 mm/min; then, the strain was released at the same speed, and when the strain amount became 0%, a holding time of 100 s was used to eliminate the residual strain. With the above as one cycle, the deformation was applied for 10 cycles, and the reflection spectrum was measured at every 2.5% strain.

4.2.14. Uniaxial Elongation Test. A uniaxial extension test was performed using a dumbbell-shaped test piece. A small bench tester (EZ-Test, Shimadzu) was used. A test piece was prepared by cutting an elastomer sheet with a thickness of 1 mm to ISO37-4 using a Super dumbbell cutter (SDMP-1000-D) (Figure S22). Two black seals were attached to the neck portion of the dumbbell-shaped test piece, which was then attached to the jig on the tensile tester so as not to loosen. The distance between the jigs before the start of measurement was set to approximately 20 mm, and the relationship between the stress and strain before fracture was obtained by stretching at a rate of 6 mm/

min at room temperature. The strain was detected using a video-type noncontact extensometer (TRViewX manufactured by Shimadzu Corp.) attached to a tensile tester and following the intervals of the seals attached to the test pieces. The tensile test was conducted at least three times under the same conditions (Figures S30–S35). In addition, changes in the Poisson's ratio in the film width direction and the film thickness direction due to uniaxial stretching were also measured.

4.2.15. Hysteresis Measurement. The energy dissipation rate of the elastomer caused by the deformation was determined. The test piece was cut according to ISO37-4 in the same manner as for the uniaxial extension test. The test piece was attached to a dynamic viscoelasticity measuring device (TA instrument, RSA-G1) so that the distance between the jigs was 20 mm, and a predetermined amount of strain was applied at room temperature at an extension speed of 6 mm/min. Later, the strain was canceled at the same speed to obtain a hysteresis loop curve. The applied strain amount was increased from 50 to 300% in steps of 50%. In the uniaxial extension test, the displacement of the neck part of the dumbbell-shaped test piece was followed by the camera, but in this test, only the displacement between the jigs could be read. Therefore, first, the difference between the deformation rate of the neck part obtained by the camera and the deformation rate between the jigs was obtained from the results of the uniaxial extension testing of pMEO₂MA, pMEO₂MA–SiO₂ (180–23.4), and pMEO₂MA–SiO₂ (180–44.9). By doing so, the amount of deformation between the jigs was determined (Figure S44 and Table S6). The hysteresis loss rate is the ratio of the stress–strain curve area during the loading process to the stress–strain curve area during the unloading process (Figures S45–S53).

4.2.16. Energy Recovery Rate Measurement. The energy recovery rate of the test piece was obtained by mounting the test piece, which was completely relaxed after applying a predetermined amount of strain, on the tensile tester again and performing a uniaxial elongation test. Since the initial length between the marks was different when elongating the test piece with residual strain, the calculation formula described below was used when obtaining the area of the stress–strain curve.

The second extension test was performed after it was confirmed that there was no further change in the size of the sample after the first extension. In the second uniaxial elongation test, the test was carried out with the same conditions as in the first test, with the residual strain sample attached to the tester. However, for TRviewX to read the mark, the test piece must be attached without slack. Therefore, the stress–strain curves obtained from the first and second uniaxial elongation tests were standardized with different initial lengths. This is shown schematically in Figure S24.

When the initial gauge length of the test piece was l_0 , the gauge distance for residual strain R_s was l_1 , the gauge distance for the first maximum extension was l_2 , and the same gauge distance was extended the second time. The strain ϵ'_{\max} was calculated using the maximum strain ϵ_{\max} given in the first time.

$$\epsilon'_{\max} = \frac{l_2 - l_1}{l_1} \frac{1 - R_s}{1 + R_s \times \epsilon_{\max}} \times \epsilon_{\max} \quad (5)$$

The area of the first stress–strain curve was calculated by

$$W_1 = \int_0^{\epsilon_{\max}} \sigma_1 d\epsilon \quad (6)$$

On the other hand, for the area of the second stress–strain curve, the area from 0 to ϵ'_{\max} was obtained, but since the strain was standardized by l_1 , it was expanded to l_1/l_0

$$W_2 = \frac{l_1}{l_0} \times \int_0^{\epsilon'_{\max}} \sigma_2 d\epsilon \quad (7)$$

The ratio of W_2 and W_1 was defined as the energy recovery rate (Figures S58–S68).

■ ASSOCIATED CONTENT

SI Supporting Information

The Supporting Information is available free of charge at <https://pubs.acs.org/doi/10.1021/acsapm.0c00703>.

Physical property information of silica fine particles (Tables S1, S2, and S3); conceptual diagram of the measurement method of the reflection spectrum and the scattering spectrum (Figure S1); angular dependence of scattering spectra of MEO₂MA and MEO₂MA solution in which silica particles are suspended (Figures S2–S4); optical photographs of MEO₂MA and MEO₂MA solution in which silica particles are suspended (Figures S5, S6, S9, and S10); dependence of the reflection spectrum of the MEO₂MA solution in which silica particles are suspended on the amount of silica particles (Figures S7, S8, S11, and S12); conceptual diagram of the cell used to prepare the elastomer (Figure S13); optical photograph of MEO₂MA and the elastomer composed of silica particles and MEO₂MA (Figures S14–S17); results of thermogravimetric analysis of MEO₂MA and the elastomer composed of silica particles and MEO₂MA (Figure S18 and Table S4); wavelength dependence of the refractive index of the polymer composed of MEO₂MA, MEO₂MA (pMEO₂MA), and silica particles (Figure S19); conceptual diagram of the measuring method of the transmission spectrum and the reflection spectrum of the elastomer (Figures S20, S21); conceptual diagram of the shape of the elastomer used in the mechanical test (Figure S22); evaluation method for the tear test (Figure S23); explanation of residual strain of the elastomer (Figure S24); effect of cross-link density on the stress–strain curve of the elastomer (Figures S25, S26); changes in the arrangement of silica particles when the composite elastomer is uniaxially stretched (Figures S27, S28); method for measuring the Poisson's ratio of the elastomer (Figure S29); elastomer stress–strain test results (Figures S30–S39); elastomer tear test results (Figures S40–S43 and Table S5); relationships among the test time, strain, and stroke strain (Figures S44 and Table S6); elastomer hysteresis test results (Figures S45–S54); results of residual strain test of the elastomer (Figures S55–S57); results of the stress–strain test on repeated elongation of the elastomer (Figures S58–S66); hysteresis loss ratios and nonrecoverable energy dissipation ratios for the elastomers (Figures S67–S68); energy recovery ratios for the pMEO₂MA and pMEO₂MA–SiO₂ elastomers (Figure S69) (PDF)

■ AUTHOR INFORMATION

Corresponding Author

Yukikazu Takeoka – Department of Molecular & Macromolecular Chemistry, Nagoya University, Nagoya 464-8603, Japan; orcid.org/0000-0002-1406-0704; Email: ytakeoka@chembio.nagoya-u.ac.jp

Authors

Eiji Miwa – Department of Molecular & Macromolecular Chemistry, Nagoya University, Nagoya 464-8603, Japan

Kenta Watanabe – Department of Molecular & Macromolecular Chemistry, Nagoya University, Nagoya 464-8603, Japan

Fumio Asai – Department of Molecular & Macromolecular Chemistry, Nagoya University, Nagoya 464-8603, Japan; Research & Development Center, Unitika Ltd, Uji-Shi, Kyoto 611-0021, Japan; orcid.org/0000-0002-2690-1187

Takahiro Seki – Department of Molecular & Macromolecular Chemistry, Nagoya University, Nagoya 464-8603, Japan; orcid.org/0000-0003-3010-2641

Kenji Urayama – Department of Macromolecular Science & Engineering, Kyoto Institute of Technology, Kyoto 606-8585, Japan; orcid.org/0000-0002-2823-6344

Jérémy Odent – Laboratory of Polymeric and Composite Materials, Center of Innovation and Research in Materials and Polymers, University of Mons, 7000 Mons, Belgium; orcid.org/0000-0002-3038-846X

Jean-Marie Raquez – Laboratory of Polymeric and Composite Materials, Center of Innovation and Research in Materials and Polymers, University of Mons, 7000 Mons, Belgium; orcid.org/0000-0003-1940-7129

Complete contact information is available at: <https://pubs.acs.org/doi/10.1021/acsapm.0c00703>

Notes

The authors declare no competing financial interest.

■ ACKNOWLEDGMENTS

This work was supported by Unitika Ltd.

■ REFERENCES

- (1) Garcés, J. M.; Moll, D. J.; Bicerano, J.; Fibiger, R.; McLeod, D. G. Polymeric nanocomposites for automotive applications. *Adv. Mater.* **2000**, *12*, 1835–1839.
- (2) Bokobza, L. The reinforcement of elastomeric networks by fillers. *Macromol. Mater. Eng.* **2004**, *289*, 607–621.
- (3) Ding, H. B.; Liu, C. H.; Ye, B. F.; Fu, F. F.; Wang, H.; Zhao, Y. J.; Gu, Z. Z. Free-Standing Photonic Crystal Films with Gradient Structural Colors. *ACS Appl. Mater. Interfaces* **2016**, *8*, 6796–6801.
- (4) Ding, T.; Cao, G. S.; Schäfer, C. G.; Zhao, Q. B.; Gallei, M.; Smoukov, S. K.; Baumberg, J. J. Revealing Invisible Photonic Inscriptions: Images from Strain. *ACS Appl. Mater. Interfaces* **2015**, *7*, 13497–13502.
- (5) Fudouzi, H.; Sawada, T. Photonic rubber sheets with tunable color by elastic deformation. *Langmuir* **2006**, *22*, 1365–1368.
- (6) Furumi, S.; Fudouzi, H.; Miyazaki, H. T.; Sakka, Y. Flexible polymer colloidal-crystal lasers with a light-emitting planar defect. *Adv. Mater.* **2007**, *19*, 2067–2072.
- (7) Ito, T.; Katsura, C.; Sugimoto, H.; Nakanishi, E.; Inomata, K. Strain-Responsive Structural Colored Elastomers by Fixing Colloidal Crystal Assembly. *Langmuir* **2013**, *29*, 13951–13957.
- (8) Liu, F.; Shan, B.; Zhang, S. F.; Tang, B. T. SnO₂ Inverse Opal Composite Film with Low-Angle-Dependent Structural Color and Enhanced Mechanical Strength. *Langmuir* **2018**, *34*, 3918–3924.
- (9) Meng, Y.; Tang, B. T.; Ju, B. Z.; Wu, S. L.; Zhang, S. F. Multiple Colors Output on Voile through 3D Colloidal Crystals with Robust Mechanical Properties. *ACS Appl. Mater. Interfaces* **2017**, *9*, 3024–3029.
- (10) Park, T. J.; Hwang, S. K.; Park, S.; Cho, S. H.; Park, T. H.; Jeong, B.; Kang, H. S.; Ryu, D. Y.; Huh, J.; Thomas, E. L.; Park, C. Electrically Tunable Soft-Solid Block Copolymer Structural Color. *ACS Nano* **2015**, *9*, 12158–12167.
- (11) Tan, H. Y.; Lyu, Q. Q.; Xie, Z. J.; Li, M. M.; Wang, K.; Wang, K.; Xiong, B. J.; Zhang, L. B.; Zhu, J. T. Metallo-supramolecular Photonic Elastomers with Self-Healing Capability and Angle-Independent Color. *Adv. Mater.* **2019**, *31*, No. 1805496.
- (12) Lee, G. H.; Han, S. H.; Kim, J. B.; Kim, D. J.; Lee, S.; Hamonangan, W. M.; Lee, J. M.; Kim, S.-H. Elastic Photonic

Microbeads as Building Blocks for Mechanochromic Materials. *ACS Appl. Mater. Interfaces* **2020**, *2*, 706–714.

(13) Lee, G. H.; Choi, T. M.; Kim, B.; Han, S. H.; Lee, J. M.; Kim, S.-H. Chameleon-Inspired Mechanochromic Photonic Films Composed of Non-Close-Packed Colloidal Arrays. *ACS Nano* **2017**, *11*, 11350–11357.

(14) Fudouzi, H.; Xia, Y. N. Photonic papers and inks: Color writing with colorless materials. *Adv. Mater.* **2003**, *15*, 892–896.

(15) Holtz, J. H.; Asher, S. A. Polymerized colloidal crystal hydrogel films as intelligent chemical sensing materials. *Nature* **1997**, *389*, 829–832.

(16) Watanabe, K.; Miwa, E.; Asai, F.; Seki, T.; Urayama, K.; Nakatani, T.; Fujinami, S.; Hoshino, T.; Takata, M.; Liu, C.; Mayumi, K.; Ito, K.; Takeoka, Y. Highly Transparent and Tough Filler Composite Elastomer Inspired by the Cornea. *ACS Mater. Lett.* **2020**, *2*, 325–330.

(17) Gent, A. N.; Tobias, R. H. Threshold Tear Strength of Elastomers. *J. Polym. Sci., Polym. Phys. Ed.* **1982**, *20*, 2051–2058.

(18) Edwards, D. C. Polymer-Filler Interactions in Rubber Reinforcement. *J. Mater. Sci.* **1990**, *25*, 4175–4185.

(19) Fukahori, Y. The mechanics and mechanism of the carbon black reinforcement of elastomers. *Rubber Chem. Technol.* **2003**, *76*, 548–565.

(20) Van Meegen, W.; Pusey, P. N.; Bartlett, P. Phase-Behavior of Dispersions of Hard Spherical-Particles. *Phase Transitions* **1990**, *21*, 207–227.

(21) Prum, R. O.; Torres, R. H.; Williamson, S.; Dyck, J. Coherent light scattering by blue feather barbs. *Nature* **1998**, *396*, 28–29.

(22) Takeoka, Y.; Yoshioka, S.; Takano, A.; Arai, S.; Nueangnoraj, K.; Nishihara, H.; Teshima, M.; Ohtsuka, Y.; Seki, T. Production of Colored Pigments with Amorphous Arrays of Black and White Colloidal Particles. *Angew. Chem., Int. Ed.* **2013**, *52*, 7261–7265.

(23) Nakamura, H.; Ishii, M. Effects of compression and shearing on the microstructure of polymer-immobilized non-close-packed colloidal crystalline arrays. *Langmuir* **2005**, *21*, 11578–11581.

(24) Kanai, T.; Sawada, T.; Yamanaka, J. Fabrication of large-area silica colloidal crystals immobilized in hydrogel film. *J. Ceram. Soc. Jpn.* **2010**, *118*, 370–373.

(25) Iwata, M.; Teshima, M.; Seki, T.; Yoshioka, S.; Takeoka, Y. Bio-Inspired Bright Structurally Colored Colloidal Amorphous Array Enhanced by Controlling Thickness and Black Background. *Adv. Mater.* **2017**, *29*, No. 1605050.

(26) Ge, D. T.; Yang, L. L.; Wu, G. X.; Yang, S. Angle-independent colours from spray coated quasi-amorphous arrays of nanoparticles: combination of constructive interference and Rayleigh scattering. *J. Mater. Chem. C* **2014**, *2*, 4395–4400.

(27) Michael Rubinstein, R. H. C. *Polymer Physics*; Oxford, 2003.

(28) Urayama, K.; Takigawa, T.; Masuda, T. Poisson Ratio of Poly(Vinyl Alcohol) Gels. *Macromolecules* **1993**, *26*, 3092–3096.

(29) Takeoka, Y. Angle-independent structural coloured amorphous arrays. *J. Mater. Chem.* **2012**, *22*, 23299–23309.

(30) *The Science and Technology of Rubber*; 4th ed.; Academic Press, 2013.

(31) Odent, J.; Raquez, J.-M.; Dubois, P.; Giannelis, E. P. Ultra-stretchable ionic nanocomposites: from dynamic bonding to multi-responsive behavior. *J. Mater. Chem. A* **2017**, *5*, 13357–13363.

(32) Odent, J.; Wallin, T. J.; Pan, W. Y.; Kruemplestaedter, K.; Shepherd, R. F.; Giannelis, E. P. Highly Elastic, Transparent, and Conductive 3D-Printed Ionic Composite Hydrogels. *Adv. Funct. Mater.* **2017**, *27*, No. 1701807.

(33) Potaufeu, J.-E.; Odent, J.; Notta-Cuvier, D.; Delille, R.; Barrau, S.; Giannelis, E. P.; Lauro, F.; Raquez, J. M. Mechanistic insights on ultra-tough polylactide-based ionic nanocomposites. *Compos. Sci. Technol.* **2020**, *191*, No. 108075.